



HAL
open science

Electronic Structure and Triplet-Triplet Energy Transfer in Artificial Photosynthetic Antennas

Marely E. Tejeda-Ferrari, Chelsea L. Brown, Gabriela C. C. C. Coutinho,
Ghabriel A. Gomes De Sa, Julio L. Palma, Manuel J. Llansola-Portoles,
Gerdenis Kodis, Vladimiro Mujica, Junming Ho, Devens Gust, et al.

► **To cite this version:**

Marely E. Tejeda-Ferrari, Chelsea L. Brown, Gabriela C. C. C. Coutinho, Ghabriel A. Gomes De Sa, Julio L. Palma, et al. Electronic Structure and Triplet-Triplet Energy Transfer in Artificial Photosynthetic Antennas. *Photochemistry and Photobiology*, 2019, 95 (1), pp.211–219. 10.1111/php.12979 . hal-02174910

HAL Id: hal-02174910

<https://hal.science/hal-02174910>

Submitted on 18 Nov 2020

HAL is a multi-disciplinary open access archive for the deposit and dissemination of scientific research documents, whether they are published or not. The documents may come from teaching and research institutions in France or abroad, or from public or private research centers.

L'archive ouverte pluridisciplinaire **HAL**, est destinée au dépôt et à la diffusion de documents scientifiques de niveau recherche, publiés ou non, émanant des établissements d'enseignement et de recherche français ou étrangers, des laboratoires publics ou privés.

1 **Electronic Structure and Triplet-Triplet Energy Transfer in** 2 **Artificial Photosynthetic Antennas**

3 Marely E. Tejeda-Ferrari¹, Chelsea L. Brown¹, Gabriela C. C. Coutinho¹, Ghabriel
4 A. Gomes de Sá¹, Julio L. Palma², Manuel J. Llansola-Portoles³, Gerdenis Kodis¹,
5 Vladimiro Mujica¹, Junming Ho*⁴,
6 Devens Gust*¹, Thomas A. Moore*¹, Ana L. Moore¹*

8 ¹. School of Molecular Sciences, Arizona State University, Tempe, AZ 85287, USA,

9 ². Department of Chemistry, The Pennsylvania State University, Fayette, The Eberly Campus,
10 Lemont Furnace, PA 15456, USA, ³. Institute for Integrative Biology of the Cell (I2BC), CEA,

11 CNRS, Université Paris-Saclay, F-91198, Gif-sur-Yvette cedex, France, ⁴. School of
12 Chemistry, University of New South Wales, Sydney, NSW 2052, Australia.

13 *Corresponding authors e-mail: junming.ho@unsw.edu.au (Junming Ho)

14 gust@asu.edu (Devens Gust), tmoore@asu.edu (Thomas A. Moore),

15 amoore@asu.edu (Ana L. Moore)

17 **ABSTRACT**

18 Three Pd(II) phthalocyanine–carotenoid dyads featuring chromophores linked by amide bonds
19 were prepared in order to investigate the rate of triplet-triplet (T-T) energy transfer from the
20 tetrapyrrole to the covalently attached carotenoid as a function of the number of conjugated
21 double bonds in the carotenoid. Carotenoids having 9, 10 and 11 conjugated double bonds were
22 studied. Transient absorption measurements show that intersystem crossing in the Pd(II)
23 phthalocyanine takes place in 10 ps in each case and that T-T energy transfer occurs in 126 ps,
24 81 ps and 132 ps in the dyads bearing 9, 10 and 11 double bond carotenoids, respectively. To
25 identify the origin of this variation in T-T energy transfer rates, density functional theory (DFT)
26 was used to calculate the T-T electronic coupling in the three dyads. According to the
27 calculations, the primary reason for the observed T-T energy transfer trend is larger T-T
28 electronic coupling between the tetrapyrrole and the 10-double bond carotenoid. A methyl
29 group adjacent to the amide linker that connects the Pd(II) phthalocyanine and the carotenoid in
30 the 9 and 11-double bond carotenoids is absent in the 10-double bond carotenoid, and this
31 difference alters its electronic structure to increase the coupling.

32

33 INTRODUCTION

34 In photosynthetic organisms, solar energy is collected by light-harvesting complexes and the
35 excitation energy is transferred to reaction centers, where it is converted into electrochemical
36 potential by charge separation (1). The key light-harvesting molecules in these complexes are
37 chlorophylls (tetrapyrroles), but carotenoids are also present as accessory antenna pigments.
38 Carotenoids harvest light in the blue/green region of the visible spectrum where chlorophylls
39 have low absorptivity. Additionally, because of the large structural variability of carotenoids
40 their spectral properties can be tuned to optimize the fitness of an organism for a particular
41 ecological niche (2-4).

42 In photosynthesis carotenoids not only act as antenna molecules, but also play a central
43 role in photoregulation and photoprotection (5-7). When a photosynthetic organism is exposed
44 to high light conditions, carotenoids photoregulate by dissipating excess singlet excitation
45 energy in the form of heat through non-photochemical quenching (NPQ) by at least three types
46 of mechanisms (5, 7-10). Photoprotection by carotenoids is another vital process that operates
47 in all photosynthetic organisms and has been studied for decades. When a singlet excited state
48 is formed in a chlorophyll, it can undergo intersystem crossing (ISC) to the triplet state, which
49 is a potent sensitizer of singlet oxygen. Singlet oxygen is a reactive oxygen species and is one
50 of the most dangerous chemical species for cellular components (6, 11-13). It has been
51 determined that when the chlorophyll and carotenoid interchromophore distance is very short
52 (essentially van der Waals contact), triplet-triplet (T-T) energy transfer from the chlorophyll to
53 the carotenoid takes place. This process reduces the lifetime of the chlorophyll triplet state by
54 many orders of magnitude, rendering it kinetically incompetent to sensitize singlet oxygen (14,

55 15). The energy of the triplet excited state of the carotenoids lies below that of singlet oxygen
56 (0.97 eV) and hence it cannot sensitize singlet oxygen, and decays harmlessly to the ground state
57 (12, 6). It is well-known that in purple bacteria bacteriochlorophyll-to-carotenoid T-T energy
58 transfer occurs on the nanosecond time scale (20-200 ns) (16). This process is relatively slow
59 compared to that in the light-harvesting complex II (LHCII) of higher plants, where it has not
60 been precisely measured but it is known to be much faster than the singlet chlorophyll lifetime
61 of ~3 ns (12). Such fast T-T transfer has not only been measured in plant LHCII, but also in the
62 peridinin-chlorophyll protein (17) and fucoxanthin-chlorophyll protein of algae, (18, 19)
63 suggesting that it is conserved in oxygenic photosynthesis. It has been postulated that such
64 ultrafast quenching of the triplet state of chlorophylls is an example of a molecular
65 photoprotective adaptation that took place during the evolution of oxygenic photosynthesis (20).

66 It is important to understand the photoprotective mechanisms extant in nature in order to
67 adapt them to improve the functionality and lifespan of reengineered photosynthesis and other
68 artificial photosynthetic systems. Indeed, to sustainably meet human needs for food, fuel and
69 biomass photosynthesis could/must be reengineered to produce up to a ca. 10-fold increase in
70 biomass yield, which will result in a concomitant increase in O₂ production. As mentioned
71 above, studies of photoprotection in bacteria and higher plants suggest that evolutionary
72 processes provide levels of photoprotection in response to ambient O₂ levels. Although a sudden
73 large increase in O₂ production in a reengineered photosynthetic plant would not be expected to
74 increase ambient O₂ levels, it could transiently increase local levels in the thylakoid membranes
75 close to the oxygen-evolving complex and nearby chlorophylls resulting in photodamage due to
76 singlet oxygen sensitization. To avoid this possibility, a much higher level of photoprotection
77 could be initially engineered into the improved photosynthetic systems. This requires an atomic

78 level understanding of the parameters controlling tetrapyrrole-carotenoid interactions.
79 Importantly, these interactions control light harvesting, photoregulation and photoprotection and
80 the factors controlling these three separate functions must be identified in order to resolve the
81 apparent paradox that the same or similar carotenoids can provide both light harvesting and
82 photoregulation, which are contradictory functions (21-23).

83 To contribute to a fundamental understanding of T-T energy transfer mechanisms
84 relevant to photosynthesis, we have designed and prepared a series of bio-inspired dyads
85 consisting of carotenoids of different conjugation lengths (9, 10, and 11 double bonds) and a
86 phthalocyanine linked by an amide group. The amide was chosen due to its proven stability and
87 because it provides good electronic coupling between carotenoids and phthalocyanines (5, 8, 9,
88 24). The phthalocyanine has been metallated with palladium in order to use the heavy atom
89 effect to increase the rate of ISC (25). Because the two chromophores absorb in different regions
90 of the visible spectrum, selective excitation of the phthalocyanine moiety followed by fast ISC
91 to form its triplet state in high yield is possible. Thus, measurement of the rate of the subsequent
92 T-T energy transfer to the carotenoid is facilitated.

93 **MATERIALS AND METHODS**

94 **General analytical:** Steady state UV-visible spectra were obtained with a Shimadzu UV-
95 2559 UV-visible spectrophotometer. Mass spectrometry was performed with a Voyager DE-
96 STR matrix-assisted laser desorption/ionization time-of-flight spectrometer (MALDI-TOF),
97 equipped with a 60 Hz laser, using (1E, 3E)-1,4-diphenylbuta-1,3-diene (DPB) as a matrix. The
98 reported mass is that of the most abundant isotope observed. The ¹H-NMR spectra were taken

99 on a Varian spectrometer at 400 MHz. Samples were prepared using deuterated solvents
100 containing 0.03% tetramethylsilane as an internal standard.

101 **Time resolved fluorescence:** Fluorescence decay measurements were performed by the
102 time-correlated single-photon-counting method. The excitation source was a fiber
103 supercontinuum laser based on a passive mode locked fiber laser and a high-nonlinearity
104 photonic crystal fiber supercontinuum generator (Fianium SC450). The laser provides 6-ps
105 pulses at a repetition rate variable between 0.1 and 40 MHz. The laser output was sent through
106 an acousto-optical tunable filter (Fianium AOTF) to obtain excitation pulses at desired
107 wavelengths in the ca. 450-900 nm region. Fluorescence emission was detected at the magic
108 angle using a double grating monochromator (Jobin Yvon Gemini-180) and a microchannel
109 plate photomultiplier tube (Hamamatsu R3809U-50). The instrument response function was 35-
110 55 ps. The spectrometer was controlled by software based on the LabView programming
111 language and data acquisition was done using a single photon counting card (Becker-Hickl,
112 SPC-830). The data analysis was carried out using locally written software (ASUFIT)
113 developed in the MATLAB environment (Mathworks Inc.). Data were fitted as a sum of
114 exponential decays which were reconvoluted with the appropriate instrument response function.
115 Goodness of fit was established by examination of residuals and the reduced χ^2 value.

116 **Transient absorption:** Femtosecond to nanosecond transient absorption measurements were
117 acquired with a 1 kilohertz pulsed laser source and a pump-probe optical setup. Laser pulses at
118 800 nm (c.a. 100 fs) were generated from an amplified, mode-locked titanium sapphire kilohertz
119 laser system (Millennia/Tsunami/Spitfire, Spectra Physics). Part of the laser pulse energy was
120 sent through an optical delay line and focused onto a 3 mm sapphire plate to generate a white

121 light continuum for the probe beam. The remainder of the pulse energy was used to pump an
122 optical parametric amplifier (Spectra Physics) to generate excitation pulses at 700 nm, which
123 were selected using a mechanical chopper. The white light probe beam was compressed by
124 prism pairs (CVI) before passing through the sample. The polarization of the pump beam was
125 set to the magic angle (54.7°) relative to the probe beam and its energy was adjusted to 200 nJ
126 using a continuously variable neutral density filter. The beams were focused in a 2 mm path-
127 length quartz cuvette to a ~ 400 μm diameter spot. The white light probe was dispersed by a
128 spectrograph (300 line grating) onto a charge-coupled device (CCD) camera (DU420, Andor
129 Tech.). The final spectral resolution was about 2.3 nm for over a nearly 300 nm spectral region.
130 The instrument response function was ca. 100 fs. The decay-associated spectra (DAS) were
131 obtained by fitting globally the transient absorption kinetic traces over a selected wavelength
132 region simultaneously as described by equation (1) (parallel kinetic model) (26), where $\Delta A(\lambda, t)$

$$\Delta A(\lambda, t) = \sum_{i=1}^n A_i(\lambda) \exp(-t/\tau_i) \quad (1)$$

134 is the observed absorption change at a given wavelength at time delay t and n is the number of
135 kinetic components used in the fitting. A plot of $A_i(\lambda)$ versus wavelength is called a Decay
136 Associated Spectra (DAS) and represents the amplitude spectrum of the i th kinetic component,
137 which has a lifetime of τ_i . Random errors associated with the reported lifetimes obtained from
138 transient absorption measurements were typically $\leq 5\%$.

139 **Synthesis:** The 4-hexanamidophthalonitrile was synthesized following a previously published
140 method (5). The carotenoid esters, methyl 8'-apo- β -caroten-8'-oate (9 double bonds), methyl 6'-
141 apo- β -caroten-6'-oate (10 double bonds), and methyl 4'-apo- β -caroten-4'-oate (11 double

142 bonds), were prepared as described before (27, 28) and the corresponding acids were obtained
143 by base promoted hydrolysis.

144 ***Pd(II) 8,11,15,18,22,25-hexabutoxy-2-hexanamidophthalocyanine (Pc):*** Portions of 4-
145 hexanamidophthalonitrile (456 mg, 1.89 mmol), 3,6-dibutoxyphthalonitrile (1.50 g, 5.67 mmol),
146 and PdCl₂ (603 mg, 3.40 mmol) were dissolved in 30 mL of butanol, heated to 45 °C, and flushed
147 with argon for 15 min. A portion of 1,8-diazabicyclo[5.4.0]undec-7-ene (DBU, 3.39 ml) was
148 added and the solution was heated to 118 °C. The reflux was kept overnight under a blanket of
149 argon. The green mixture was cooled to room temperature and 100 mL of a water/chloroform
150 mixture (1:1) was added. The organic layer was extracted, dried over Na₂SO₄, and filtered. The
151 solvent was concentrated by rotary evaporation. The product was purified by column
152 chromatography (silica gel, 1% MeOH/10% ethyl acetate/CHCl₃). Pd(II) 8,11,15,18,22,25-
153 hexabutoxy-2-hexanamidophthalocyanine was obtained in 1.05 % yield (23 mg). ¹H-NMR δ
154 ppm (20% Pyridine-d/CDCl₃): 1.09 (t, J = 7.4, 7.4 Hz, 3H), 1.27 (m, 18H), 1.70 (m, 4H), 2.24
155 (q, 2H), 2.39 (t, J = 7.5, 7.5 Hz, 2H), 3.20-5.20 (m, 36H), 6.85 (d, J = 8.7 Hz, 1H), 7.13 (d, J =
156 8.8 Hz, 1H), 7.38 (d, J = 9.6 Hz, 1H), 7.52 (d, J = 9.3 Hz, 1H), 7.64 (m, 2H), 8.31 (d, J = 7.8 Hz,
157 1H), 9.26 (d, J = 7.9 Hz, 1H), 10.03 (s, 1H), 10.84 (s, 1H). MALDI-TOF: m/z obsd. 1163.46
158 calc. for C₆₂H₇₅N₉O₇Pd 1163.48. UV/vis λ_{max} (95% CHCl₃/5% MeOH): 327, 647, and 721
159 nm.

160 ***Pd(II) 2-amino-8,11,15,18,22,25-hexabutoxyphthalocyanine:*** The hexamido-
161 phthalocyanine obtained in the above reaction (20.4 mg, 17.6 μmol) was dissolved in 10 mL of
162 tetrahydrofuran (THF) and 5 mL of a saturated methanolic solution of KOH. The solution was
163 heated to 65°C and stirred overnight. The reaction mixture was diluted with chloroform and
164 washed with water (three times). The organic layer was dried over Na₂SO₄ and filtered, and the
165 solvent was removed by rotary evaporation. The desired Pd(II) 2-amino-8,11,15,18,22,25-
166 hexabutoxyphthalocyanine (18.5 mg) was obtained in 99 % yield. MALDI-TOF: m/z obsd.

167 1065.32 calc. for $C_{56}H_{65}N_9O_6Pd$ 1065.41. UV/vis λ_{max} (95% $CHCl_3$ /5% MeOH): 324, 647,
168 and 721 nm.

169 **Dyad-9:** The 8'-apo- β -caroten-8'-oic acid (28.5 mg, 65.7 μ mol) and Pd(II) 2-amino-
170 8,11,15,18,22,25-hexabutoxyphthalocyanine (35 mg, 32.9 μ mol) were dissolved in 45 mL of
171 dry chloroform. While under argon, 1-ethyl-3-(3-dimethylaminopropyl)carbodiimide (EDCI,
172 68.9 mg, 0.36 mmol) and 4-dimethylaminopyridine (224 mg, 1.83 mmol) were added. The
173 reaction was stirred overnight at room temperature under a blanket of argon. The solvent was
174 removed by rotary evaporation and the product was purified by column chromatography (silica,
175 2% MeOH/dichloromethane). The product was then purified by two preparative TLCs, the first
176 in 1% MeOH/5% ethyl acetate/chloroform and the second in 2% MeOH/dichloromethane.
177 **Dyad-9** (5.7 mg) was obtained in 12 % yield. 1H -NMR δ ppm (5% pyridine- d / $CDCl_3$): 0.68
178 (m, 6H), 0.88 (m, 18H), 1.02 (m, 4H), 1.10 (m, 6H), 1.18 (s, 2H), 1.65 (m, 15H), 1.98 (m, 6H),
179 2.30 (m, 12H), 4.98 (m, 12H), 6.21-6.85 (m, 11H), 7.11 (d, $J = 9.0$ Hz, 1H), 7.37 (m, 1H), 7.51
180 (m, 1H), 7.71 (m, 1H), 8.04 (d, $J = 8.1$ Hz, 1H), 8.45 (d, $J = 9.3$ Hz, 1H), 9.22 (s, 2H), 9.44 (s,
181 1H), 9.62 (s, 1H), 10.14 (s, 1H). MALDI-TOF: m/z obsd. 1479.98 calc. for $C_{86}H_{103}N_9O_7Pd$
182 1479.70. UV/vis λ_{max} (95% $CHCl_3$ /5% MeOH): 330, 454, 648, and 722 nm.

183 **Dyad-10:** It was prepared by the same procedure described for **dyad-9** except using 6'-apo- β -
184 caroten-6'-oic acid (6.8 mg, 18% yield). 1H -NMR δ ppm (5% pyridine- d / $CDCl_3$): 0.68 (m, 6H),
185 0.88 (m, 18H), 1.02 (m, 4H), 1.10 (m, 6H), 1.18 (s, 2H),), 1.65 (m, 15H), 1.98 (m, 6H), 2.30
186 (m, 12H), 4.98 (m, 12H), 6.05-6.87 (m, 13H), 7.07 (d, $J = 12.1$ Hz, 1H), 7.50 (m, 1H), 7.60 (m,
187 1H), 7.71 (m, 1H), 8.04 (d, $J = 8.2$ Hz, 1H). 8.38 (s, 1H), 9.22 (s, 2H), 9.67 (s, 1H), 9.74 (s,
188 1H), 9.95 (s, 1H). MALDI-TOF: m/z obsd. 1505.70 calc. for $C_{88}H_{105}N_9O_7Pd$ 1505.72. UV/vis
189 λ_{max} (95% $CHCl_3$ /5% MeOH): 327, 470, 650, and 725 nm.

190 **Dyad-11:** It was prepared by the same procedure described for **dyad-9** except using 4'-apo- β -
191 caroten-4'-oic acid (8.1 mg, 9.8% yield). 1H -NMR δ ppm (5% pyridine- d / $CDCl_3$): 0.68 (m,

192 6H), 0.88 (m, 18H), 1.02 (m, 4H), 1.10 (m, 6H), 1.18 (s, 2H), 1.65 (m, 15H), 1.98 (m, 6H), 2.30
 193 (m, 12H), 4.98 (m, 12H), 6.05-6.88 (m, 15H), 7.07 (d, J = 10.4 HZ, 1H), 7.46 (d, 1H), 7.52 (m,
 194 1H), 7.60 (m, 2H), 8.38 (s, 1H), 8.52 (d, J = 8.1 Hz, 1H), 8.93 (s, 1H), 9.23 (d, J = 7.9 Hz, 1H),
 195 9.48 (s, 1H), 9.55 (s, 1H). MALDI-TOF: m/z obsd. 1545.83 calc. for C₉₁H₁₀₉N₉O₇Pd 1545.75.
 196 UV/vis λ_{max} (95% CHCl₃/5% MeOH): 330, 482, 649, and 723 nm.

197 **Computational details:** All electronic structure calculations were carried out using the
 198 Gaussian 09 (29) and Q-CHEM programs (30). The geometries of the dyads were optimized
 199 using the dispersion corrected (B3LYP+GD3BJ) (31, 32) and with 6-31G(d) basis set specified
 200 for all atoms, except Pd, where the lanl2dz basis set was used. The triplet-triplet coupling was
 201 computed using the fragment excitation difference (FED) (33) method implemented in Q-
 202 CHEM, (30) and these were evaluated at the TD-B3LYP/6-31G(d) level (employing the Tamm-
 203 Dancoff approximation). The expression for the FED method is shown in equation (2).

$$204 \quad V = \frac{(E_2 - E_1)|\Delta x_{12}|}{\sqrt{(\Delta x_{11} - \Delta x_{22}) + 4\Delta x_{12}^2}} \quad (2)$$

205 $\Delta E = (E_2 - E_1)$ is the difference in energies of the porphyrin and the carotenoid triplet states
 206 defined by (Por(S0)-Car(T1) and Por(T1)-Car(S0)); the $|\Delta x_{12}|$ term measures the extent of
 207 delocalization of the excited states calculated by subtracting the appropriated electron densities
 208 on the acceptor and donor fragments (34). The boundary between the donor and acceptor
 209 fragments is defined to be at the C–N amide bond. Ideally, the energies should be evaluated on
 210 Por(T1)-Car(S0) geometry, i.e., after ISC. For **dyad-9'**, we found that the RMSD between the
 211 Por(T1)-Car(S0) and Por(S0)-Car(S0) optimized geometries is 0.06 Å. Accordingly in the
 212 present work, we made an approximation by carrying out FED calculations on the ground state
 213 geometries, Por(S0)-Car(S0) (See Fig. S2 in Supplementary Materials).

214 **RESULTS**215 **Synthesis**

216 The synthesis of the Pd(II) phthalocyanine (**Pc**) was achieved by the condensation reaction of
217 4-hexanamidophthalonitrile (**5**) and 3,6-dibutoxyphthalonitrile, in the presence of PdCl₂. Those
218 reagents were heated to reflux in butanol in the presence of 1,8-diazabicyclo[5.4.0]undec-7-ene
219 (DBU) to yield the statistical mixture of phthalocyanines. Thin layer chromatography (TLC) of
220 the reaction crude showed four main products: the less polar Pd(II) 1,4,8,11,15,18,22,25-
221 octabutoxyphthalocyanine side product, the desired phthalocyanine, **Pc**, the more polar Pd(II)
222 15,18,22,25-tetrabutoxy-2,9-dihexanamidophthalocyanine and its regioisomeric side products,
223 and the very polar Pd(II) 22,25-dibutoxy-2,9,16-trihexanamidophthalocyanine and its
224 regioisomeric side products. The polarity differences between the products allowed separation
225 using silica column chromatography to yield **Pc** (1% yield). The amide group of **Pc** was
226 hydrolyzed under basic conditions to form Pd(II) 2-amino-8,11,15,18,22,25-
227 hexabutoxyphthalocyanine (99% yield). To prepare the dyads, the carboxylic acid carotenoids
228 of various double bond conjugation lengths (9, 10, and 11 double bonds) were synthesized
229 following a previously published procedure (27). The coupling of the carboxylic acid
230 carotenoids to the aminophthalocyanine was done in chloroform using 1-ethyl-3-(3-
231 dimethylaminopropyl)carbodiimide hydrochloride (EDCI) as the coupling reagent with 4-
232 dimethylaminopyridine (DMAP) as the base. Each dyad was purified using silica column
233 chromatography and multiple preparative TLCs to give **dyad-9** in 12% yield, **dyad-10** in 18%
234 yield, and **dyad-11** in 10% yield (Fig. 1).

235

<Figure 1>

236 **Steady-state absorption**

237 Fig. 2 shows the absorption spectra of **dyad-9**, **dyad-10**, **dyad-11**, and the reference **Pc** in
238 toluene. The absorption band with maximum around ~320 nm corresponds to the Soret band of
239 **Pc** and the bands with maxima at ~640 nm and 720 nm correspond to the **Pc** Q bands. The broad
240 absorption bands between ~400 and 550 nm are associated primarily with the carotenoid
241 absorption and, as expected, shift to the red with increasing conjugation length. The spectra of
242 the individual dyes are minimally perturbed by forming the dyads.

243 <Figure 2>

244 **Time resolved fluorescence**

245 Time-resolved fluorescence measurements for **dyad-10** show fast (~10 ps) decay of the **Pc**
246 singlet excited state (see Supplementary Materials, Fig. S1); similar results were obtained for
247 the other dyads and model **Pc** (not shown). The decay of the phthalocyanine first excited singlet
248 state on this short time scale is ascribed mainly to formation of the corresponding phthalocyanine
249 triplet state, as shown by the transient absorption results discussed below.

250 **Transient absorption spectroscopy**

251 In order to further elucidate the fate of the excited singlet state of the **Pc** in the dyads, transient
252 absorption measurements were performed for the three dyads and **Pc**. As mentioned before,
253 carotenoids have no absorption in the 700 nm region and above. Therefore it is possible to
254 selectively excite just the phthalocyanine moiety of a dyad at 700 nm. Global analysis of the
255 transient absorption data obtained upon 700 nm excitation of **Pc** and for the three dyads
256 dissolved in toluene gave the decay-associated spectra (DAS) shown in Fig. 3. For **Pc**, four

257 DAS with time constants of 0.5 ps, 11 ps, 90 ps, and a non-decaying (on the 1 ns time scale)
258 component are associated with the decay of the **Pc** excited state. The 11 ps DAS shows the
259 decay of the **Pc** singlet excited state forming **³Pc** (ISC) with appearance of the triplet excited
260 state induced absorption at around 600 nm. The 0.5 ps DAS and 90 ps DAS are associated with
261 the relaxation/solvation of the **Pc** singlet and triplet excited states, respectively. The 0.5 ps DAS
262 shows the characteristic derivative like feature (positive amplitude on the red side of the
263 bleaching band and negative amplitude on the blue side) corresponding to the red shift and
264 increase of the Q band bleaching at ~710 nm due to relaxation/solvation. The non-decaying
265 DAS is associated with **³Pc**, and shows the characteristic induced absorption at around 600 nm
266 and Q band bleaching at ~710 nm.

267 <Figure 3>

268 Global analysis of the transient absorption data for **dyad-9** gave four DAS with time
269 constants of 2 ps, 10 ps, 126 ps, and a non-decaying component (Fig. 3 b). The 2 ps component
270 in this and the other dyads is associated with the relaxation/solvation of the **Pc** singlet excited
271 state. The 10 ps DAS is associated with the decay of the **Pc** singlet-excited state to form **³Pc**
272 (ISC), because it shows the formation/rise (negative amplitude) of the induced absorption at
273 around 625 nm. The 126 ps DAS corresponds to T-T energy transfer between **³Pc** and the
274 carotenoid to yield triplet carotenoid (**³Car**), and it shows the rise of the induced absorption
275 characteristic of the **³Car** at around 530 nm and simultaneous decay of the ground state
276 bleaching at ~710 nm associated with **³Pc** returning to the ground state. The non-decaying DAS
277 is due to **³Car**, which eventually decays to the ground state. Note that this DAS also shows a
278 bleaching band at ~710 nm associated with the **Pc**. This phenomenon is a characteristic of

279 strongly coupled carotenoid-tetrapyrrole systems and its presence has been known for a long
280 time, but its origin is not well understood (35, 36). These results indicate that the T-T energy
281 transfer from the ^3Pc to the triplet excited state of the 9-double bond carotenoid in **dyad-9** occurs
282 with a time constant of 126 ps.

283 For **dyad-10** the global analysis of the transient absorption data gave four DAS with time
284 constants of 2 ps, 10 ps, 81 ps, and a non-decaying component (Fig. 3 c). Similar to **dyad-9**, the
285 10 ps DAS is associated with the formation of ^3Pc (ISC). The 81 ps DAS in **dyad-10**
286 corresponds to the T-T energy transfer from ^3Pc to yield ^3Car , again because the characteristic
287 ^3Car induced absorption at around 550 nm grows in (negative amplitude), while simultaneously
288 the decay of the ground state bleaching of ^3Pc at 710 nm is observed. These results indicate that
289 the T-T energy transfer from the ^3Pc to the 10-double bond carotenoid triplet in **dyad-10** occurs
290 in 81 ps, which is faster than for **dyad-9**. As before, the non-decaying DAS is associated with
291 the decay of ^3Car . In **dyad-11** the picture is similar to that of **dyad-9** with DAS of 2ps, 10 ps,
292 132 ps, and a non-decaying component (Fig. 3 d). The 132 ps DAS in **dyad-11** corresponds to
293 T-T energy transfer from ^3Pc to yield ^3Car .

294 <Figure 4>

295 **Theoretical calculations**

296 Theoretical computations were performed in an attempt to determine the structural basis for the
297 trend in the experimental rates of T-T energy transfer from the phthalocyanine to the appended
298 carotenoids in the dyads. For purposes of computation, models of **dyad-9**, **dyad-10** and **dyad-**
299 **11**, indicated as **dyad-9'**, **dyad-10'** and **dyad-11'**, were generated. Note that in the

322 monotonically as the carotenoid chain length increases. Analysis of the individual contributions
323 to the electronic coupling (see Table S2, Supplementary Materials) indicates that longer
324 conjugated carotenoid chains lead to a larger ΔE (the carotenoid triplet becomes lower in
325 energy), and the resulting triplet excited states also become more localized on the polyene
326 (smaller $|\Delta x_{12}|$). As shown in equation (2), the coupling depends strongly on the two effects (ΔE
327 and $|\Delta x_{12}|$), which appears to be acting in opposite directions in these systems (the denominator
328 has a value around 4 for all the dyads – see Table S2). Comparison with **dyads-9'**, **dyad-10'**
329 and **dyad-11'** (see Table S1, Supplementary Materials) further indicates that the non-methylated
330 carotenoids lead to an increased energy difference between the donor-acceptor triplet states
331 (larger ΔE) and that appears to be the origin of the larger coupling values for these model dyads.
332 In addition, the optimized geometries of **dyad-9''**, **dyad-10''** and **dyad-11''** display carotenoid
333 conformations that are linearly extended, whilst the carotenoids in **dyads-9'**, **dyad-10'** and
334 **dyad-11'** are significantly curved (see Figure 6) (38). To investigate the effect of this
335 geometrical difference, T-T couplings were computed on *partially optimized* geometries of
336 **dyad-9''**, **dyad-10''** and **dyad-11''** where the carotenoid chain is constrained to the geometries
337 in **dyads-9'**, **dyad-10'** and **dyad-11'**. As shown in Table 1 (see values in parentheses), the
338 curvature in the carotenoid chain attenuates the T-T coupling. This suggests that the origin of
339 the trend in T-T coupling for **dyads-9'**, **dyad-10'** and **dyad-11'** may be due to a geometrical
340 effect induced by the presence of methyl groups on the carotenoid backbone.

341 <Figure 6>

342 To examine the effect of the methyl group adjacent the amide linkage, we considered the
343 computational models **dyad-9'''**, **dyad-10'** and **dyad-11'''** where a hydrogen atom was

344 substituted for a methyl group in the case of **dyad-9'''** and **dyad-11'''** (the methyl group is not
345 present in this position in **dyad-10'**). The results clearly indicate that absence of the adjacent
346 methyl group in **dyad-9'''** and **dyad-11'''** increases the magnitude of the T-T energy transfer
347 coupling compared with **dyad-9'** and **dyad-11'** (see Table 1). The origin of this trend is in the
348 $|\Delta x_{12}|$ term (see Table S1 and S3, Supplementary Materials). The similarity in T-T transfer
349 coupling in **dyad-9''**, **dyad-10''** and **dyad-11''** indicates that the adjacent methyl group exerts a
350 particularly strong influence.

351 <Table 1>

352 In summary, these calculations suggest that the presence of a methyl group adjacent to
353 the amide linkage leads to triplet states that are more localized and consequently have smaller
354 coupling values as observed in **dyad-9'** and **dyad-11'**. In addition, there appears to be a
355 geometrical effect induced by the presence of methyl groups on the carotenoid backbone.

356 DISCUSSION

357 The experimental data show that for all three dyads, the phthalocyanine singlet state formed
358 upon excitation rapidly decays by ISC to give the phthalocyanine triplet and by other pathways.
359 The phthalocyanine triplet then decays by T-T transfer to produce the carotenoid triplet state.
360 The time constants for the T-T transfer are 126 ps, 81 ps and 132 ps for **dyad-9**, **dyad-10** and
361 **dyad-11**, respectively (Fig. 4). If we make the reasonable assumption that increasing the
362 carotenoid chain length increases the thermodynamic driving force for T-T transfer and
363 concurrently the spectral overlap, (27) we would expect that the rate of T-T transfer would
364 increase as the number of double bonds in the carotenoid increases. Clearly, this is not the case.

365 In addition to thermodynamic effects, electronic coupling also plays an important role in
366 determining T-T transfer rates. We therefore undertook theoretical calculations in order to
367 determine values for carotenoid-phthalocyanine electronic coupling for each dyad, and for some
368 relevant computational structures. First-principle DFT calculations show that the electronic
369 coupling promoting T-T energy transfer for **dyad-10** is stronger than those for **dyad-9** and **dyad-**
370 **11**, which is in agreement with the kinetic measurements. The calculations indicate that
371 carotenoids having a methyl group adjacent to the amide linkage (as in **dyad-9** and **dyad-11**)
372 lead to triplet states that are more localized and consequently have smaller coupling values than
373 those of carotenoids lacking such methyl groups, as in **dyad-10**. Our calculations also suggest
374 that conformational changes (a slight S-shape in the carotenoid) due to the presence of the
375 methyl groups along the carotenoid backbone must also be considered a factor in increasing the
376 coupling in **dyad-10** over that in **9** and **11**. We therefore associate the change in coupling due to
377 methyl groups acting in two ways. There is an intrinsic effect of the methyl group near the
378 amide bond on the electronic structure of the triplet state, which gives rise to the observed
379 changes in T-T transfer rates. There is also a change in the electronic structure of the triplet
380 state due to a conformational change driven by the methyl groups along the carotenoid backbone,
381 which increases the T-T transfer rate in **dyad-10**.

382 CONCLUSIONS

383 In this work we directly determined T-T transfer rates in model systems mimicking oxygenic
384 photosynthesis and demonstrated that T-T transfer rates are much faster than the natural ISC rate
385 and tetrapyrrole singlet lifetime, which is a prerequisite for effective triplet state quenching of
386 the tetrapyrrole and prevention of singlet oxygen sensitization. The experimental and theoretical

387 investigation of T-T transfer in a set of three carotenoid-phthalocyanine dyads shows that the
388 transfer rate is a function of the electronic coupling via the linkage joining the carotenoid and
389 phthalocyanine.

390 Relatively small changes in carotenoid structure near this linkage have discernable
391 effects on T-T transfer rates. Because antenna function (S-S energy transfer), photoprotection
392 (T-T energy transfer) and photoregulation (S-S energy transfer, electron transfer and excitonic
393 coupling) (8) by carotenoids in artificial photosynthetic constructs and in photosynthesis are
394 functions of the electronic coupling between the two chromophores, the results of this study
395 suggest that a detailed understanding of the electronic coupling is an important design feature
396 of artificial photosynthetic systems that incorporate carotenoid and tetrapyrrole chromophores.
397 It is important to define structures in which those features of the electronic coupling that would
398 favor the desired process, light harvesting or photoregulation, can be identified. Taken together,
399 light harvesting and photoregulation make up an apparent energy wasting futile cycle. In fact,
400 such cycles are known in metabolic pathways where they play a crucial role in regulating
401 metabolic flux to maintain near constant ATP chemical potential in response to changing
402 bioenergetic demands on the cell, (39) but they are not known to play such roles in the primary
403 photophysics of photosynthesis.

404

405 **ACKNOWLEDGMENTS:** This research was supported by the U.S. Department of
406 Energy, Office of Science, Office of Basic Energy Sciences, under Award DE-FG02-
407 03ER15393. JH acknowledges the Australian Research Council for financial support (Grant
408 No. DE160100807) and the Australian NCI and Intersect Australia Ltd for generous allocation
409 of computational resources.

410 **SUPPLEMENTARY MATERIALS**

411 Figure S1, Table S1–S3 and the cartesian coordinates of the DFT optimized geometries can be
412 found at DOI: 10.1562/2006-xxxxxx.s1.

413

414 **REFERENCES**

415 1. Blankenship, R. E. (2014) *Molecular mechanisms of photosynthesis* Wiley Blackwell,
416 Oxford, UK, NJ, USA.

417 2. Polívka, T. and H. A. Frank (2010) Molecular factors controlling photosynthetic light
418 harvesting by carotenoids. *Acc. Chem. Res.* **43**, 1125-1134.

419 3. Croce, R. and H. van Amerongen (2014) Natural strategies for photosynthetic light
420 harvesting. *Nat. Chem. Biol.* **10**, 492-501.

421 4. Fuciman, M., G. Keşan, A. M. LaFountain, H. A. Frank and T. Polívka (2015) Tuning
422 the spectroscopic properties of aryl carotenoids by slight changes in structure. *J. Phys. Chem. B*
423 **119**, 1457-1467.

424 5. Berera, R., C. Herrero, I. H. M. van Stokkum, M. Vengris, G. Kodis, R. E. Palacios, H.
425 van Amerongen, R. van Grondelle, D. Gust, T. A. Moore, A. L. Moore and J. T. M. Kennis
426 (2006) A simple artificial light-harvesting dyad as a model for excess energy dissipation in
427 oxygenic photosynthesis. *Proc. Natl. Acad. Sci. U. S. A.* **103**, 5343-5348.

428 6. Frank, H. A. and R. J. Cogdell (1996) Carotenoids in photosynthesis. *Photochem.*
429 *Photobiol.* **63**, 257-264.

- 430 7. Holt, N. E., D. Zigmantas, L. Valkunas, X.-P. Li, K. K. Niyogi and G. R. Fleming (2005)
431 Carotenoid cation formation and the regulation of photosynthetic light harvesting. *Science* **307**,
432 433-436.
- 433 8. Kloz, M., S. Pillai, G. Kodis, D. Gust, T. A. Moore, A. L. Moore, R. van Grondelle and
434 J. T. M. Kennis (2011) Carotenoid photoprotection in artificial photosynthetic antennas. *J. Am.*
435 *Chem. Soc.* **133**, 7007-7015.
- 436 9. Berera, R., I. H. M. van Stokkum, G. Kodis, A. E. Keirstead, S. Pillai, C. Herrero, R. E.
437 Palacios, M. Vengris, R. van Grondelle, D. Gust, T. A. Moore, A. L. Moore and J. T. M. Kennis
438 (2007) Energy transfer, excited-state deactivation, and exciplex formation in artificial caroteno-
439 phthalocyanine light-harvesting antennas. *J. Phys. Chem. B* **111**, 6868-6877.
- 440 10. Staleva, H., J. Komenda, M. K. Shukla, V. Šlouf, R. Kaňa, T. Polívka and R. Sobotka
441 (2015) Mechanism of photoprotection in the cyanobacterial ancestor of plant antenna proteins.
442 *Nat. Chem. Biol.* **11**, 287-291.
- 443 11. Polívka, T. and V. Sundström (2004) Ultrafast dynamics of carotenoid excited
444 states—from solution to natural and artificial systems. *Chem. Rev.* **104**, 2021-2072.
- 445 12. Gall, A., R. Berera, M. T. A. Alexandre, A. A. Pascal, L. Bordes, M. M. Mendes-Pinto,
446 S. Andrianambinintsoa, K. V. Stoitchkova, A. Marin, L. Valkunas, P. Horton, J. T. M. Kennis,
447 R. van Grondelle, A. Ruban and B. Robert (2011) Molecular adaptation of photoprotection:
448 Triplet states in light-harvesting proteins. *Biophys. J.* **101**, 934-942.

- 449 13. Foote, C. S. (1976) Photosensitized oxidation and singlet-oxygen: Consequences in
450 biological systems. In *Free radicals in biology*, Vol. 2. (Edited by W. A. Pryor). Academic
451 Press, New York.
- 452 14. Monger, T. G., R. J. Cogdell and W. W. Parson (1976) Triplet states of
453 bacteriochlorophyll and carotenoids in chromatophores of photosynthetic bacteria. *Biochim.*
454 *Biophys. Acta, Bioenerg.* **449**, 136-153.
- 455 15. Mathis, P., W. L. Butler and K. Satoh (1979) Carotenoid triplet state and chlorophyll
456 fluorescence quenching in chloroplasts and subchloroplast particles. *Photochem. Photobiol.* **30**,
457 603-614.
- 458 16. Angerhofer, A., F. Bornhauser, A. Gall and R. J. Cogdell (1995) Optical and optically
459 detected magnetic-resonance investigation on purple photosynthetic bacterial antenna
460 complexes. *Chem. Phys.* **194**, 259-274.
- 461 17. Bonetti, C., M. T. A. Alexandre, R. G. Hiller, J. T. M. Kennis and R. van Grondelle
462 (2009) Chl-a triplet quenching by peridinin in H-PCP and organic solvent revealed by step-scan
463 FTIR time-resolved spectroscopy. *Chem. Phys.* **357** 63-69.
- 464 18. Papagiannakis, E., I. H. M. van Stokkum, H. Fey, C. Büchel and R. van Grondelle (2005)
465 Spectroscopic characterization of the excitation energy transfer in the fucoxanthin–chlorophyll
466 protein of diatoms. *Photosynth. Res.* **86**, 241-250.
- 467 19. Khoroshyy, P., D. Bina, Z. Gardian, R. Litvín, J. Alster and J. Pšenčík (2018) Quenching
468 of chlorophyll triplet states by carotenoids in algal light-harvesting complexes related to
469 fucoxanthin-chlorophyll protein. *Photosynth. Res.* **135**, 213-225.

- 470 20. Ho, J., E. Kish, D. D. Mendez-Hernandez, K. WongCarter, S. Pillai, G. Kodis, J. Niklas,
471 O. G. Poluektov, D. Gust, T. A. Moore, A. L. Moore, V. S. Batista and B. Robert (2017) Triplet-
472 triplet energy transfer in artificial and natural photosynthetic antennas. *Proc. Natl. Acad. Sci. U.*
473 *S. A.* **114**, E5513-E5521.
- 474 21. Gust, D., T. A. Moore and A. L. Moore (2009) Solar fuels via artificial photosynthesis.
475 *Acc. Chem. Res.* **42**, 1890-1898.
- 476 22. Gust, D., T. A. Moore and A. L. Moore (2012) Realizing artificial photosynthesis.
477 *Faraday Discuss.* **155**, 9-26.
- 478 23. WongCarter, K., M. J. Llansola-Portolés, G. Kodis, D. Gust, A. L. Moore and T. A.
479 Moore (2018) Light harvesting, photoregulation, and photoprotection in selected artificial
480 photosynthetic systems. In *Light harvesting in photosynthesis*. (Edited by R. v. G. R. Croce, H.
481 van Amerongen and I. van Stokkum). CRC Press. Taylor and Francis Group Boca Raton,
482 Florida.
- 483 24. Liao, P.-N., S. Pillai, D. Gust, T. A. Moore, A. L. Moore and P. J. Walla (2011) Two-
484 photon study on the electronic interactions between the first excited singlet states in
485 carotenoid–tetrapyrrole dyads. *J. Phys. Chem. A* **115**, 4082-4091.
- 486 25. Robinson, G. W. and R. P. Frosch (1963) Electronic excitation transfer and relaxation.
487 *J. Chem. Phys.* **38**, 1187-1203.
- 488 26. van Stokkum, I. H. M., D. S. Larsen and R. van Grondelle (2004) Global and target
489 analysis of time-resolved spectra. *Biochim. Biophys. Acta, Bioenerg.* **1657**, 82-104.

- 490 27. Cardoso, S. L., D. E. Nicodem, T. A. Moore, A. L. Moore and D. Gust (1996) Synthesis
491 and fluorescence quenching studies of a series of carotenoporphyrins with carotenoids of various
492 lengths. *J. Braz. Chem. Soc* **7**, 19-30.
- 493 28. Fungo, F., L. Otero, E. Durantini, W. J. Thompson, J. J. Silber, T. A. Moore, A. L.
494 Moore, D. Gust and L. Sereno (2003) Correlation of fluorescence quenching in
495 carotenoporphyrin dyads with the energy of intramolecular charge transfer states. Effect of the
496 number of conjugated double bonds of the carotenoid moiety. *Phys. Chem. Chem. Phys.* **5**, 469-
497 475.
- 498 29. Frisch, M. J., G. W. Trucks, H. B. Schlegel, G. E. Scuseria, M. A. Robb, J. R.
499 Cheeseman, G. Scalmani, V. Barone, B. Mennucci, G. A. Petersson, H. Nakatsuji, M. Caricato,
500 X. Li, H. P. Hratchian, A. F. Izmaylov, J. Bloino, G. Zheng, J. L. Sonnenberg, M. Hada, M.
501 Ehara, K. Toyota, R. Fukuda, J. Hasegawa, M. Ishida, T. Nakajima, Y. Honda, O. Kitao, H.
502 Nakai, T. Vreven, J. A. Montgomery Jr., J. E. Peralta, F. Ogliaro, M. J. Bearpark, J. Heyd, E. N.
503 Brothers, K. N. Kudin, V. N. Staroverov, R. Kobayashi, J. Normand, K. Raghavachari, A. P.
504 Rendell, J. C. Burant, S. S. Iyengar, J. Tomasi, M. Cossi, N. Rega, N. J. Millam, M. Klene, J. E.
505 Knox, J. B. Cross, V. Bakken, C. Adamo, J. Jaramillo, R. Gomperts, R. E. Stratmann, O. Yazyev,
506 A. J. Austin, R. Cammi, C. Pomelli, J. W. Ochterski, R. L. Martin, K. Morokuma, V. G.
507 Zakrzewski, G. A. Voth, P. Salvador, J. J. Dannenberg, S. Dapprich, A. D. Daniels, Ö. Farkas,
508 J. B. Foresman, J. V. Ortiz, J. Cioslowski and D. J. Fox (2009) Gaussian 09. Gaussian, Inc.,
509 Wallingford, CT, USA.
- 510 30. Shao, Y., L. F. Molnar, Y. Jung, J. Kussmann, C. Ochsenfeld, S. T. Brown, A. T. B.
511 Gilbert, L. V. Slipchenko, S. V. Levchenko, D. P. O'Neill, R. A. DiStasio Jr., R. C. Lochan, T.

- 512 Wang, G. J. O. Beran, N. A. Besley, J. M. Herbert, C. Y. Lin, T. Van Voorhis, S. H. Chien, A.
513 Sodt, R. P. Steele, V. A. Rassolov, P. E. Maslen, P. P. Korambath, R. D. Adamson, B. Austin,
514 J. Baker, E. F. C. Byrd, H. Dachsel, R. J. Doerksen, A. Dreuw, B. D. Dunietz, A. D. Dutoi, T.
515 R. Furlani, S. R. Gwaltney, A. Heyden, S. Hirata, C.-P. Hsu, G. Kedziora, R. Z. Khalliulin, P.
516 Klunzinger, A. M. Lee, M. S. Lee, W. Liang, I. Lotan, N. Nair, B. Peters, E. I. Proynov, P. A.
517 Pieniazek, Y. M. Rhee, J. Ritchie, E. Rosta, C. D. Sherrill, A. C. Simmonett, J. E. Subotnik, H.
518 L. Woodcock III, W. Zhang, A. T. Bell, A. K. Chakraborty, D. M. Chipman, F. J. Keil, A.
519 Warshel, W. J. Hehre, H. F. Schaefer III, J. Kong, A. I. Krylov, P. M. W. Gill and M. Head-
520 Gordon (2006) Advances in methods and algorithms in a modern quantum chemistry program
521 package. *Phys. Chem. Chem. Phys.* **8**, 3172-3191.
- 522 31. Becke, A. D. (1993) Density-functional thermochemistry. Iii. The role of exact
523 exchange. *J. Chem. Phys.* **98**, 5648-5652.
- 524 32. Grimme, S., S. Ehrlich and L. Goerigk (2011) Effect of the damping function in
525 dispersion corrected density functional theory. *J. Comput. Chem.* **32**, 1456-1465.
- 526 33. Hsu, C. P., Z. Q. You and H. C. Chen (2008) Characterization of the short-range
527 couplings in excitation energy transfer. *J. Phys. Chem. C* **112**, 1204-1212.
- 528 34. You, Z.-Q. and C.-P. Hsu (2014) Theory and calculation for the electronic coupling in
529 excitation energy transfer. *Int. J. Quantum Chem.* **114**, 102–115.
- 530 35. Arellano, J. B., T. B. Melo, P. K. Fyfe, R. J. Cogdell and K. R. Naqvi (2004)
531 Multichannel flash spectroscopy of the reaction centers of wild-type and mutant *rhodobacter*

532 *sphaeroides*: Bacteriochlorophyllb-mediated interaction between the carotenoid triplet and the
533 special pair. *Photochem. Photobiol.* **79**, 68-75.

534 36. Mandal, S., A.-M. Anne-Marie Carey, J. Locsin, B.-R. Gao, J. C. Williams, J. P. Allen,
535 S. Lin and N. W. Woodbury (2017) Mechanism of triplet energy transfer in photosynthetic
536 bacterial reaction centers. *J. Phys. Chem. B* **121**, 6499-6510.

537 37. You, Z.-Q. and C.-P. Hsu (2010) The fragment spin difference scheme for triplet-triplet
538 energy transfer coupling. *J. Chem. Phys.* **133**, 074105.

539 38. Fiedor, L. and M. Pilch (2018) Side methyl groups control the conformation and
540 contribute to symmetry breaking of isoprenoid chromophores. *Angew. Chem., Int. Ed. Engl.* **57**,
541 6501-6506.

542 39. Voet, D., J. G. Voet and C. W. Pratt (2016) *Fundamentals of biochemistry, life at the*
543 *molecular level*. John Wiley and Sons, Singapore.

544

545

546

547

548

549

550
551**Table 1.** Computed T-T energy transfer coupling for model dyads (in cm^{-1}).

Compound	V (cm^{-1})
Dyad-9'	11.5
Dyad-10'	13.7
Dyad-11'	8.7
Dyad-9''	19.4 (11.6) ^a
Dyad-10''	17.8 (17.5) ^a
Dyad-11''	16.5 (15.1) ^a
Dyad-9'''	16.9
Dyad-10'''	13.7
Dyad-11'''	12.6

552 ^a Model dyads with their carotenoid constrained to curved conformation in dyads-9', 10' and
553 11', respectively.

554

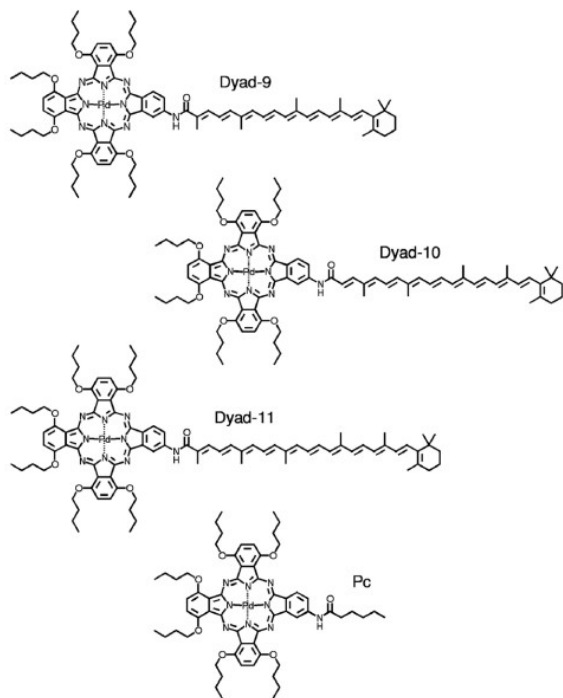
555

556

557

558

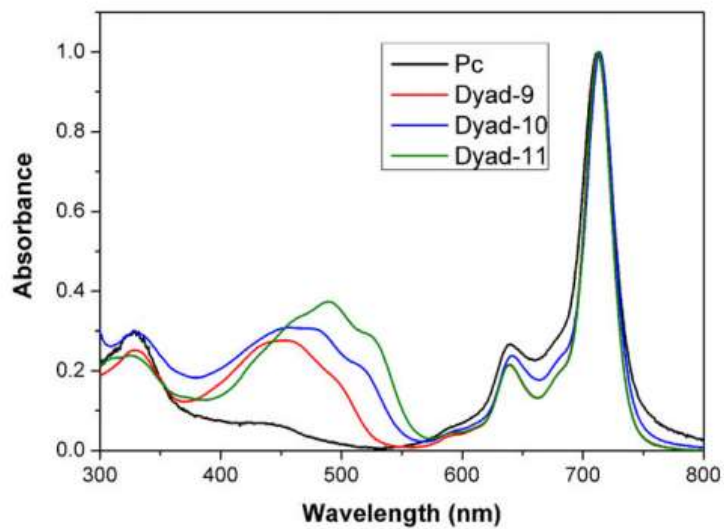
559 **FIGURES**



560

561 **Figure 1.** Molecular structures of the phthalocyanine reference (**Pc**) and
562 carotenophthalocyanine dyads with 9, 10, and 11 conjugated double bonds.

563

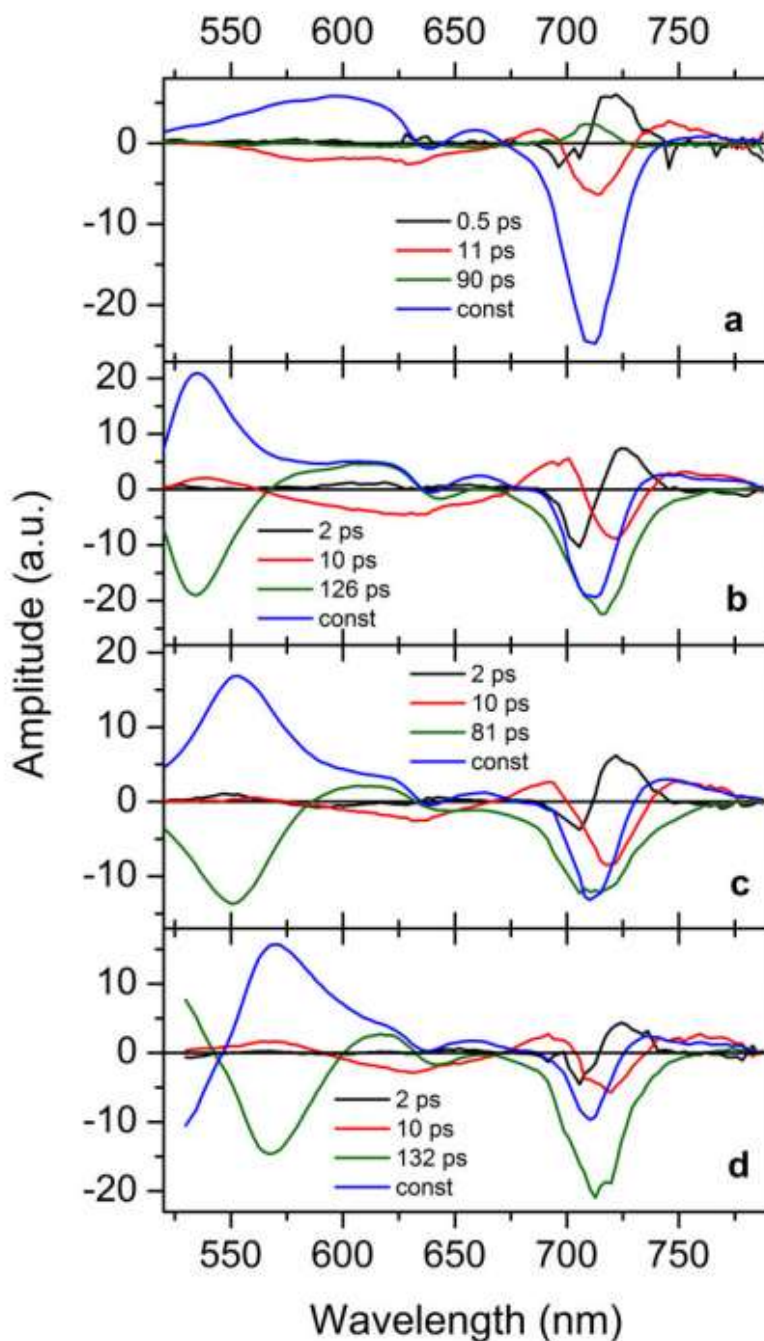


564

565 **Figure 2.** Absorption spectra in toluene of **dyad-9**, **dyad-10**, **dyad-11**, and **Pc** (black).

566

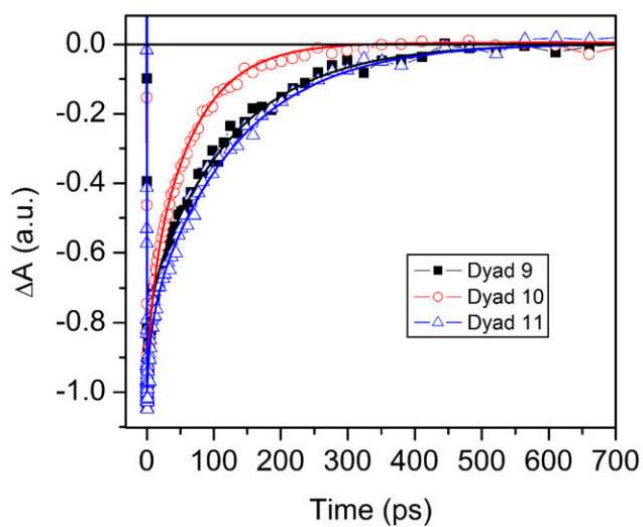
567



568

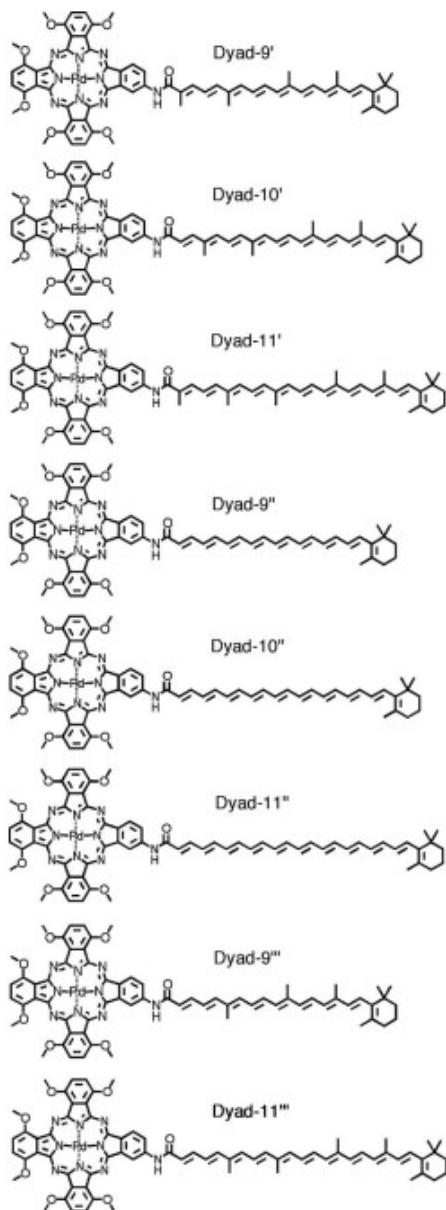
569 **Figure 3.** Decay-associated-spectra in toluene of **Pc** (a), **dyad-9** (b), **dyad-10** (c), and **dyad-**
 570 **11** (d) obtained from the transient absorption data upon excitation at 700 nm. On the 1 ns time
 571 window the ^3Pc and $^3\text{carotenoid}$ transient triplet species (^3Car) of the dyads do not decay and
 572 are shown as constants.

573



574

575 **Figure 4.** Decay kinetics and exponential fit (lines) at 710 nm for **dyad-9** (squares), **dyad-10**
576 (circles) and **dyad-11** (triangles) showing the transient absorption decay due to the T-T energy
577 transfer from **³Pc** to **³Car**. The decay kinetics has been normalized after the constant component
578 subtraction.



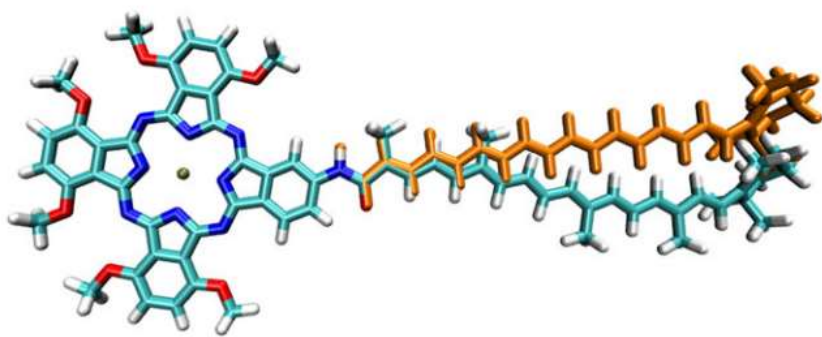
579

580 **Figure 5.** Computational models used in the determination of the T-T energy transfer coupling

581 (see Table 1).

582

583



584

585 **Figure 6.** The conformation of the carotenoid in the DFT optimized geometries of **dyad-9'** and
586 **dyad-9''** (orange).

587

588

589